Multiscale Simulations Suggest a Mechanism for the Association of the Dok7 PH Domain with PIP-Containing Membranes

Amanda Buyan, Antreas C. Kalli, Mark S. P. Sansom*

Department of Biochemistry, University of Oxford, Oxford, United Kingdom

* mark.sansom@bioch.ox.ac.uk

Abstract

Dok7 is a peripheral membrane protein that is associated with the MuSK receptor tyrosine kinase. Formation of the Dok7/MuSK/membrane complex is required for the activation of MuSK. This is a key step in the complex exchange of signals between neuron and muscle, which lead to neuromuscular junction formation, dysfunction of which is associated with congenital myasthenic syndromes. The Dok7 structure consists of a Pleckstrin Homology (PH) domain and a Phosphotyrosine Binding (PTB) domain. The mechanism of the Dok7 association with the membrane remains largely unknown. Using multi-scale molecular dynamics simulations we have explored the formation of the Dok7 PH/membrane complex. Our simulations indicate that the PH domain of Dok7 associates with membranes containing phosphatidylinositol phosphates (PIPs) via interactions of the β1/β2, β3/β4, and β5/β6 loops, which together form a positively charged surface on the PH domain and interact with the negatively charged headgroups of PIP molecules. The initial encounter of the Dok7 PH domain is followed by formation of additional interactions with the lipid bilayer, and especially with PIP molecules, which stabilizes the Dok7 PH/membrane complex. We have quantified the binding of the PH domain to the model bilayers by calculating a density landscape for protein/membrane interactions. Detailed analysis of the PH/PIP interactions reveal both a canonical and an atypical site to be occupied by the anionic lipid. PH domain binding leads to local clustering of PIP molecules in the bilayer. Association of the Dok7 PH domain with PIP lipids is therefore seen as a key step in localization of Dok7 to the membrane and formation of a complex with MuSK.

Author Summary

Neuromuscular junction formation and maintenance is an essential biological process, the disruption of which leads to congenital myasthenic syndromes and premature death. Dok7 is a key member in formation, maintenance and signaling in neuromuscular junctions. Dok7 is a peripheral membrane protein that is necessary for full activation of the receptor tyrosine kinase MuSK, a receptor tyrosine kinase residing in the postsynaptic membrane. The structure of Dok7 consists of both a PH domain and a PTB domain. The

interaction of Dok7 with cell membranes is not well understood. Here, we use molecular simulations to show that the Dok7 PH domain preferentially binds to PIP lipid molecules when associating with a membrane. Dok7 interacts with the bilayer in both a *canonical* binding mode and an *alternative* binding mode. Our simulations also demonstrate the presence of both a canonical and an atypical binding site for PIPs in agreement with recent crystallographic studies of the ASAP1 PH domain. Analysis of density landscapes for the interaction of the Dok7 PH domain with PIP-containing lipid bilayers is also able to identify both *canonical* and *alternative* binding modes. Our improved understanding of how Dok7 interacts with a membrane is key to examining Dok7/MuSK signaling.

Introduction

Dok7 (Downstream-of-Kinase 7) is a peripheral membrane protein and a member of the Dok family of proteins [1]. Dok7 is the cytoplasmic activator of muscle-specific kinase (MuSK) [2], which is involved in neuromuscular junction formation and maintenance [3–5]. Mutations in Dok7 lead to the disease *myasthenia gravis* [6–12], indicating that Dok7 plays a key role in the activation of MuSK. Dok7 contains a Pleckstrin Homology (PH) and a Phosphotyrosine Binding (PTB) domain [2], as seen in the structure: a dimer of the first 210 residues of Dok7 was co-crystallized with a phosphotyrosine-containing 13-mer peptide corresponding to the Dok7 binding site of MuSK [13]. Given that Dok7 contains a PH domain, it is likely that Dok7 may localize to cell membrane via lipid-mediated interactions (Fig 1A and 1B), but the mechanistic details of how the formation and stability of the Dok7 PH/membrane complex are as yet unknown.

PH domains are a structurally conserved family which have been shown to associate with phosphatidylinositol phosphates (PIPs; [14,15]). PH/PIP interactions help to localize PH domains to specific cellular membranes. Dok7 may interact with a number of PIP species [13], showing low micromolar affinities for (fluorescent derivatives of) PI(3,4,5)P$_3$, PI(4,5P)$_2$ and PI(3,4)P$_2$ [13]. Mutation of a positive residue (R54A) on the β3/β4 loop of the Dok7 PH domain (Fig 1B and 1C) results in a >5-fold loss of PIP binding. R54 forms part of a cluster of basic residues (with K18, K20 and R22), which form a positively charged patch on the PH domain between the unstructured regions of β1/β2 and β3/β4 strands (Fig 1C), corresponding to the *canonical* binding site for PIPs in a number of PH domains [16,17]. The PTB domain of Dok7 binds to a phosphorylated tyrosine (pTyr553) in the juxtamembrane region of MuSK, enabling downstream signalling within the cell [18,19]. It has been shown that the juxtamembrane regions of all human receptor tyrosine kinases (including MuSK) are able to interact with PIPs [20]. Thus, PIP-mediated interactions of the PH domain would be expected to aid in localization of Dok7 close to the juxtamembrane region of MuSK.

Understanding the mechanism of association of the Dok7 PH domain with a model cell membrane will provide insights into the interactions stabilizing the Dok7/MuSK/membrane complex, since the PH orientation relative to the membrane is likely to play a key role in the Dok7/MuSK interaction. It has been shown that molecular dynamics (MD) simulations provide a tool for understanding the mechanism of association of peripheral proteins with models of cell membranes [21–23], having been applied to the membrane binding interactions of e.g. PTEN [24], auxilin [25], talin [26], NRas [27,28], and the canonical PH domain of GRP1 [29]. These simulation studies have revealed specific interactions of these proteins with lipid molecules, which are in good agreement with available experimental data.
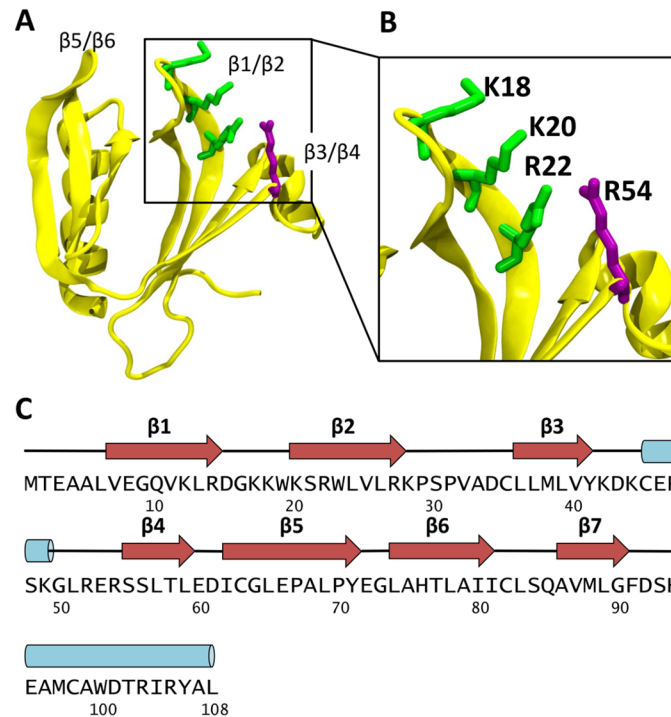
Fig 1. Previous structural studies of Dok7. (A) Structure of the PH Domain of Dok7 (PDB id: 3ML4), shown in yellow cartoon representation. **(B)** The four residues thought to be involved in PIP binding (K18, K20, R22 and R54) are in green or purple licorice representation. **(C)** The sequence of the Dok7 PH domain is shown, with the secondary structure indicated above the sequence. Black lines represent unstructured regions, red arrows represent β sheets, and blue cylinders represent α-helices.

In the current study, we employ a multi-scale MD simulation approach [21] to explore how the PH domain of Dok7 binds to model lipid bilayers with differing phospholipid and PIP contents. Our analysis employing the evaluation of interaction density landscapes is able to differentiate between *canonical* and *alternative* binding modes of the PH domain. Our results allow us to suggest a mechanism for PIP-mediated association of the PH domain of Dok7 with cell membranes.

Results

PH domain association with PIP-containing lipid bilayers

We first explored the association of the PH domain of Dok7 with a PIP-containing bilayer. In these simulations, the Dok7 PH domain was initially positioned ~7 nm away from a preformed lipid bilayer composed of 75% PC + 20% PS + 5% PIP_2. An ensemble of 20 simulations each of duration 1 μs (see Table 1) was then performed.

During each simulation, the protein diffused in the aqueous solution before interacting with the bilayer (Fig 2A). In the majority of the individual simulations within the ensembles in which PIP_2 molecules were present, the Dok7 PH domain associated with the bilayer surface within the first ~0.25 μs and remained bound for the remainder of the simulation (Fig 2B) without any dissociation events occurring. Simulations with a bilayer containing PIP_3 yielded similar results, although it took on average a little longer (~0.75 μs, see Fig 2B) for the PH domain to bind to the bilayer, despite the greater negative charge on PIP_3 compared to PIP_2. Recent experimental studies yielded dissociation constants of Dok7 (PH-PTB) for (derivatized)

Table 1. Summary of the simulations.

Simulation	Lipid Bilayer	Duration
CG-PH-pip2	PC/PS/PIP$_2$ (75%/20%/5%)	20 x 1 µs
CG-PH-pip3	PC/PS/PIP$_3$ (75%/20%/5%)	20 x 1 µs
CG-PH-pc	PC (100%)	20 x 1 µs
CG-PH-pcps	PC/PS (80%/20%)	20 x 1 µs
AT-PH-pip2	PC/PS/PIP$_2$ (75%/20%/5%)	3 x 0.3 µs
AT-PH-pip3	PC/PS/PIP$_3$ (75%/20%/5%)	3 x 0.3 µs

Summary of the simulations used in this study. The PIP$_2$ simulations used PI(4,5)P$_2$ (S1A Fig), and the PIP$_3$ simulations used PI(3,4,5)P$_3$ (S1B Fig).

doi:10.1371/journal.pcbi.1005028.t001

PIP$_2$ and PIP$_3$ of 4 and 2 µM respectively [13]. In contrast, if either a zwitterionic bilayer (100% PC) or an anionic bilayer lacking PIP (80% PC + 20% PS) is used then no association of the Dok7 PH domain with the membrane is observed (Fig 2B), in good agreement with previous studies of other PH domains [30,31]. The sample size of 20 simulations per system is smaller than those explored in e.g. recent studies of TM helix dimerization [32,33]. However, convergence analysis (S2 Fig) suggested that the density landscapes were adequately sampled close to the bilayer by 20 simulations and indeed that even with small (~5) groups of
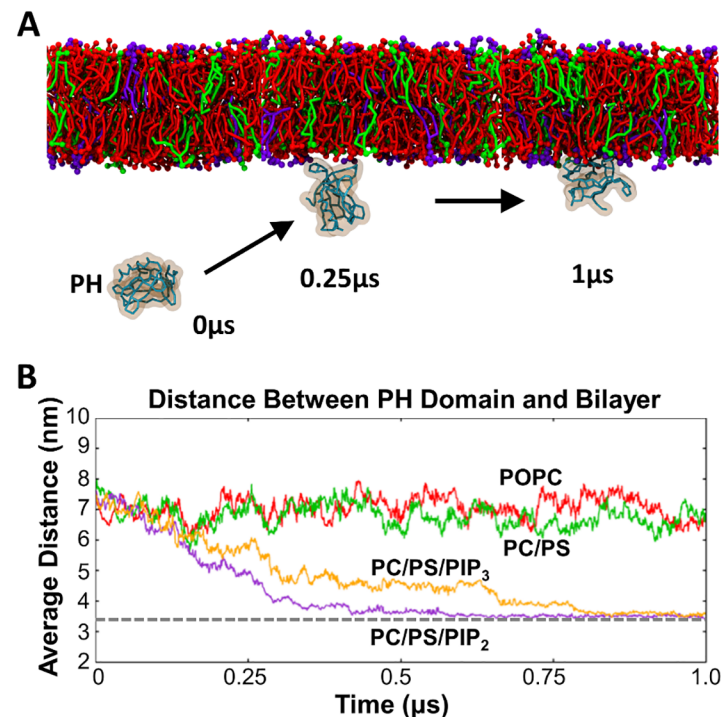
Fig 2. Simulation setup and bilayer composition dependence on binding. (A) Simulation set-up and progression. These are snapshots from a CG-PH-pip2 simulation (see Table 1 for details) at 0, 0.25 and 1 µs. PC molecules are shown in red, PS in green and PIP$_2$ molecules in purple. The PH domain of Dok7 is shown as a cyan Cα trace with orange surface. **(B)** Average distances (from the 20 simulations in each ensemble) between the centre of mass of the PH domain and that of the bilayer as a function of time are shown for four different bilayers (PC, red; PC/PS, green; PC/PS/PIP$_2$, purple; PC/PS/PIP$_3$, orange) used in the PH domain simulations. The dotted grey horizontal line indicates the approximate position of a PH domain bound to the surface of the membrane.

doi:10.1371/journal.pcbi.1005028.g002

simulations the density landscapes still resemble the overall landscape, with M1 as the predominant binding mode.

Density landscapes

To further analyse the orientation and interactions of the Dok7 PH domain relative to different lipid bilayers, we have constructed two-dimensional density landscapes of the R_{zz} component of the rotational matrix of the PH domain (R_{zz}; calculated using the g_rotmat command in GROMACS; see Methods), and of the distance of the PH domain from the bilayer (d_z). In particular, R_{zz} is the zz component of the rotational matrix required for least squares fitting of a conformation onto a reference conformation, and d_z represents the perpendicular distance between the centres of mass of the PH domain and of the lipid bilayer. R_{zz} may adopt values from -1 to +1, and is equal to +1 when we use the preferred orientation as a reference conformation for the calculation of the rotational matrix. We note that related methodologies have been used to calculate the energy landscapes e.g. of cholesterol flip-flop [34] and of the insertion of hydrophobic peptides into model membranes [35].

Analysis of the orientation of the Dok7 PH domain relative to a PIP$_2$-containing membrane reveals that there is a clearly preferred binding mode of the PH domain to the bilayer (M1 in Fig 3A). In the preferred orientation, two regions of the PH domain interact with PIP$_2$: the β1/β2 loop, which contains three cationic residues (K18, K20 and R22); and the β3/β4 loop (residues 42–54), which contains a short α-helix region at the C-terminus of which is R54 (Fig 3B). A similar preferred orientation was also observed in the density landscape for bilayers containing PIP$_3$ (M1 in Fig 3D). The alternative orientation corresponds to the minor minimum in the PIP$_2$-simulation landscape (R_{zz} = 0.2; M2 in Fig 3A—pictured in 3C for PIP$_2$, and 3F for PIP$_3$). In this orientation, the long α-helix (residues 94 to 107) of the PH domain is at an angle of ~60° relative to the plane of the bilayer, with β1/β2 and β3/β4 loops still maintaining contact with the bilayer. The M1 binding mode seen is very similar to a recently solved crystal structure of Arf GAP ASAP1 [36]. In the ASAP1 crystal structure (PBB id: 5C79), there are *two* anionic lipid binding sites: a *canonical* C-site between the β1/β2 and β3/β4 loops, and a second *atypical* A-site on the opposite face of the β1/β2 loops, towards β5/β6.

The presence of two PIP-binding sites in the ASAP1 crystal structure is very similar to the arrangement of bound PIP$_2$ molecules we see in the Dok7 simulations (Fig 4). Superimposition of the Dok7 and ASAP1 PH domains results in overlap of the headgroups of the PIP$_2$ molecules at both the C and A sites. We note in passing that in the ASAP1 crystal structure the tails of the bound dibutyryl PIP$_2$ would be pointing away from the bilayer.

To further quantify the similarities between the interactions of the Dok7 PH and ASAP1 PH domain with PIPs, 0.3 μs atomistic simulations of the Dok7 PH domain (see below) were compared to 0.5 μs simulations of the ASAP1 PH domain (the latter are described in detail in [38]). Lipid interactions for Dok7 alone (S3A Fig), ASAP1 alone (S3B Fig), and both aligned to each other (S3C Fig) show that the lipid interactions for both PH domains are similar. This observation is strengthened by quantification of the average number of contacts for both ASAP1 (S3D Fig) and Dok7 (S3E Fig). Both PH domains interact with lipids via their β1/β2 loop, as well as their β3/β4 loops, and lipids are present in both the *canonical* site, as well as the *atypical* site, in good agreement with experiments.

Evaluation of radial distribution functions (RDFs) of the different lipid species around the bound Dok7 PH domain (Fig 5) showed a large peak at 0.5 nm for PIP$_2$ and PIP$_3$, and a second peak at 1.0 nm, indicating that both PIP species preferentially cluster around the PH domain. Such clustering was not observed for PC or PS. Clustering of PIP lipids was observed only in the leaflet to which the protein was bound. Visual inspection of the simulation trajectories
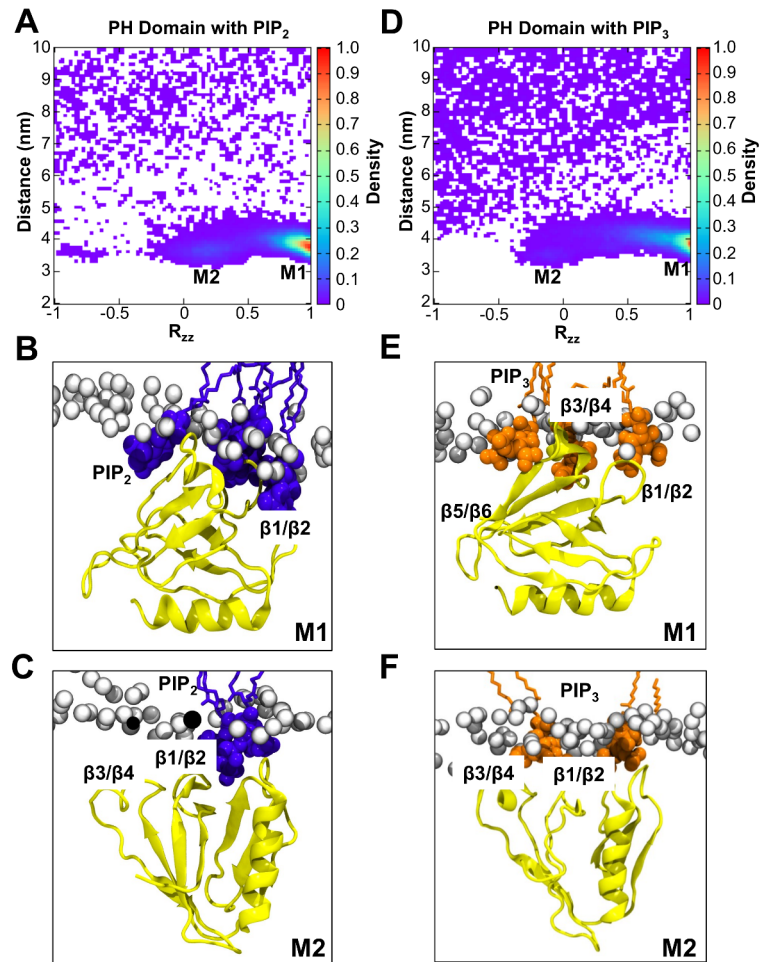
Fig 3. Density landscapes of the PH domain binding to PIP lipids. Densities of the PH domain binding to PIP$_2$ **(A)** and PIP$_3$ **(D)**. The density is shown as a function of domain orientation R$_{zz}$ and the distance between the centres of mass of the protein and the bilayer. Representative structures of the M1 orientation with PIP molecules in both the A and C sites (see main text for details), and PIP molecules that are clustered around the protein, are shown in **(B)** for PIP$_2$ and **(E)** for PIP$_3$, whilst representative structures of M2 are shown in **(C)** for PIP$_2$ and **(F)** for PIP$_3$. Note that prior to the calculation the rotation of the protein in the *xy* plane was fitted using the *trjconv* command in GROMACS [37].

doi:10.1371/journal.pcbi.1005028.g003

reveals that there are multiple PIP molecules surrounding the PH domain once it is bound to the bilayer, e.g. Fig 3B, 3C, 3E and 3F. As discussed above, the PIP lipids interact primarily with the basic residues of the β1/β2 loop and the small helix in the β3/β4, which contains R54 (see eg. Fig 6B). The main driving forces for these interactions appear to be the electrostatic interactions between the protein and the headgroups of the lipids (S4 Fig). In particular, from our analysis it seems that the protein interacts mainly with the bulky negatively charged PIP headgroups.

Atomistic simulations

The preferred (i.e. most frequently observed) orientations of the PH domain when bound to either PIP$_2$ or PIP$_3$ as identified from the CG simulations were converted to atomistic representations and multiple (3 x 0.3 μs) atomistic simulations (Table 1) were performed. During the atomistic simulations, the PH domain retained its preferred orientation relative to the bilayer,
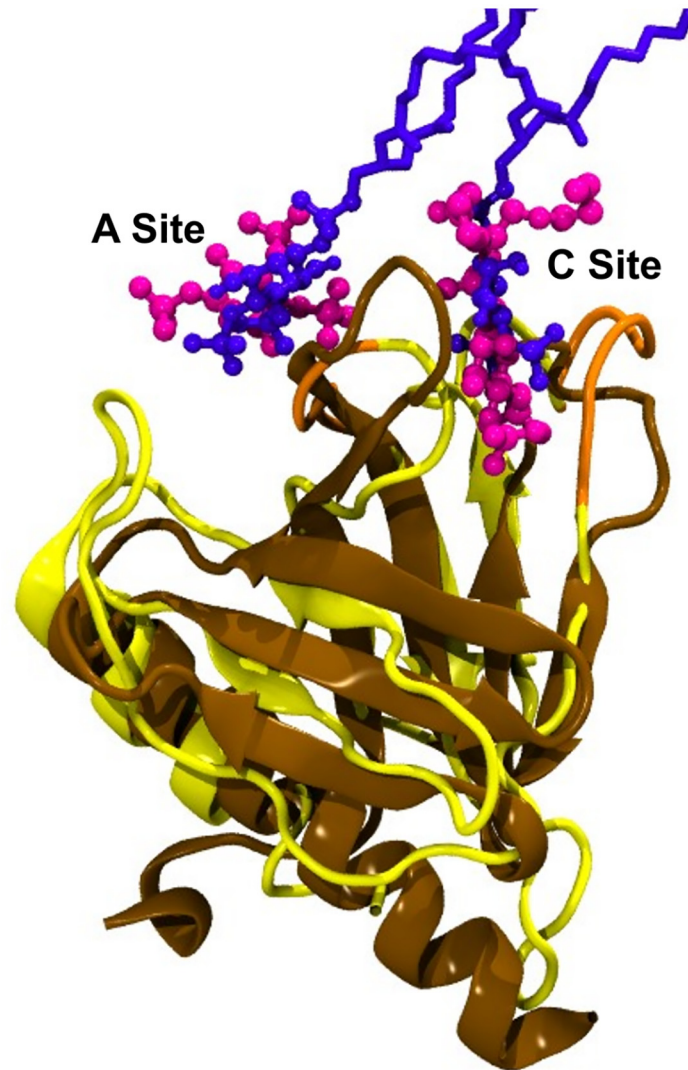
Fig 4. Comparison between the Arf GAP ASAP1 and Dok7 PH domains. Alignment of the Arf GAP ASAP1 (pdb id 5C79) with a representative structure from the simulation of the Dok7 PH domain in the presence of PIP$_2$. The Dok7 PH domain is in yellow cartoon, and the PIP$_2$ lipids from the simulation are in purple licorice and CPK. The Arf GAP ASAP1 backbone is in ochre cartoon, and the dibutyryl PIP$_2$ molecules in the crystal structure are in CPK magenta.

doi:10.1371/journal.pcbi.1005028.g004

its secondary structure (S5 Fig), and the main contacts identified from the CG-MD simulations (i.e. residues K18, K20, R22, and R54 interacting with PIP$_2$; Fig 6A and 6B). For both PIP$_2$ and PIP$_3$, in some of the simulations the number of hydrogen bonds decreased at the first ~50 ns of simulations, although PIP$_2$ maintained overall more hydrogen bonds than did PIP$_3$ (S6 Fig). Examination of the interactions at the C-site (K18, K20, R22 and R54) showed that all residues maintained approximately 1–2 hydrogen bonds, to PIP$_2$ (S7A Fig). Significantly, this was not the case for PIP$_3$, which did not maintain most hydrogen bonds at the C site over the course of the 0.3 μs simulations (S7B Fig). This suggests that Dok7 forms a more stable complex with PIP$_2$ than PIP$_3$. This is further confirmed by breaking down the interactions between the head-groups, phosphates, and tails for the atomistic simulations (S8 Fig). In this analysis, it is shown
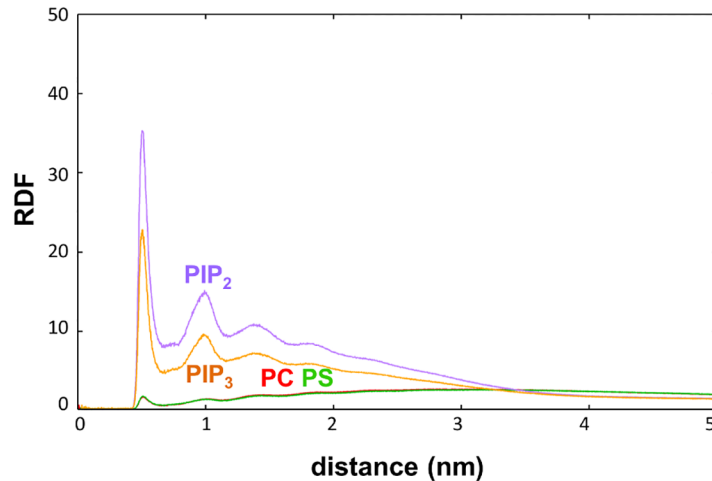
Fig 5. Average radial distribution function of PIP$_2$ and PIP$_3$ around Dok7's PH domain. The average, over the 20 repeat simulations, radial distribution function of the coarse-grained simulations with PIP lipids. Averages for the PC/PS lipids were taken from the PC/PS/PIP$_2$ simulations, whilst the PIP$_3$ line is taken from the PC/PS/PIP$_3$ simulations. The PC line is red, PS in green, PIP$_2$ in purple, and PIP$_3$ in orange.

doi:10.1371/journal.pcbi.1005028.g005
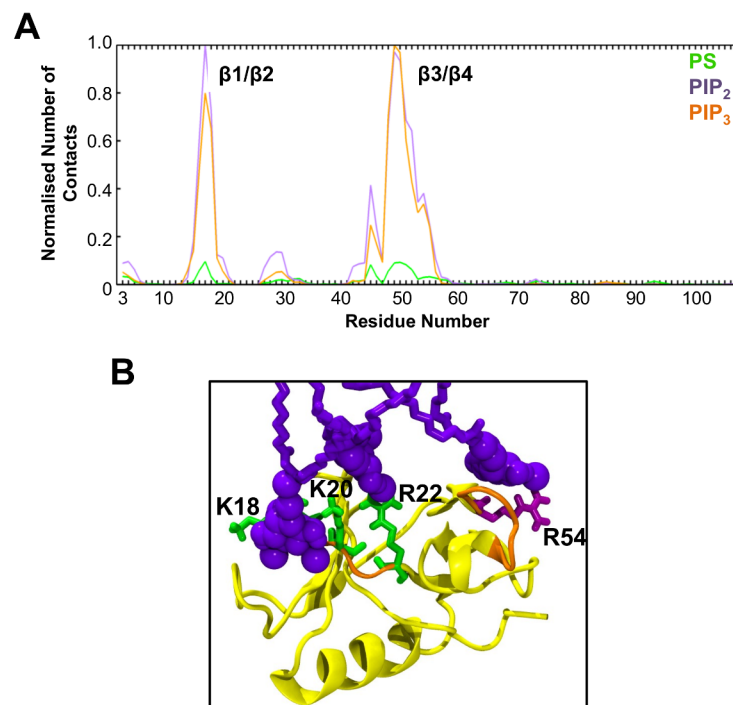
Fig 6. Lipid interactions between Dok7 and PIP$_2$/PIP$_3$. (A) Normalized interactions with PS, PIP$_2$ and PIP$_3$ as a function of residue number, derived from coarse-grained simulations. **(B)** Representative atomistic structure of the Dok7 PH domain interacting with PIPs in the bilayer. The backbone of the residues interacting with PIPs is highlighted in orange, and the main protein is in yellow cartoon. The residues proposed to interact with PIPs are shown in either green or purple licorice.

doi:10.1371/journal.pcbi.1005028.g006

that the headgroups are responsible for most of the interactions that the protein experiences, as the headgroups form the majority of the contacts between the protein and the bilayer.

Discussion

We have performed simulations of the Dok7 PH domain with complex lipid bilayers containing PIP_2 and PIP_3 molecules. Our simulations have shown that PIP molecules were needed for the formation of a stable Dok7 PH/bilayer complex. Furthermore, binding of the PH domain to the bilayer was via interactions of the β1/β2 and β3/β4 loops, i.e. in the region that was previously proposed by Bergamin et al. [13] to be the PIP binding site.

Calculation of density landscapes allowed us to quantify the Dok7 PH domain binding to the bilayer. Our analysis suggests that in the presence of PIP_2 molecules in the bilayer, the Dok7 PH domain prefers to bind in the *canonical* binding mode, similar to that seen for other PH domains [16,17,39]. When Dok7 bound to bilayers containing PIP_3, the height and width of the density in the density landscapes was a little smaller compared to that observed for binding to the PIP_2-containing bilayer. The relatively small difference in binding probabilities correlates with the observation of micromolar dissociation constants for *both* PIP_2 and PIP_3 binding to Dok7 [13]. The simulations suggest slightly weaker binding of PIP_3 than of PIP_2, whilst the experimental studies suggest slightly stronger binding of PIP_3. However, there are several differences between the simulations and the experiments respectively, namely: the protein construct (PH domain vs. Dok7); lipids used (PIPs vs. fluorescent derivatives of PIPs); and assay conditions (PIPs in a bilayer vs. in the presence of detergent). The fact that in CG simulations, Dok7 binds to both PIP_2 and PIP_3 with little apparent difference between binding probabilities, is encouraging, especially when compared to the fluorescence polarization assays. This suggests that the Dok7 PH domain may bind to both PIP_2 and PIP_3. However, *in vivo* PIP_2 is likely to be the major ligand, given its higher content in plasma membranes.

Recently, a crystal structure of the PH domain of the Arf GAP ASAP1 was solved in complex with dibutyryl-PI(4,5)P_2 lipids [36]. This provides direct structural evidence for the presence of both a canonical (C) and an atypical (A) PIP-binding site in a single PH domain. This correlates well with the two PIP-binding sites observed in our simulations (see Fig 4 and above). These two binding sites for PIP molecules on Dok7 contribute to the clustering of both PIP_2 and PIP_3 observed in our simulations. This clustering of PIP molecules may aid the association of Dok7 with the bilayer and thereby facilitate formation of a complex with MuSK.

In summary, the PH domain of Dok7 associates with the bilayer via a canonical binding mode observed for other PH domains, as evidenced by the two-dimensional density landscapes we have calculated. By virtue of possessing two binding sites for PIPs, Dok7 causes clustering of PIP lipids around it, potentially facilitating its interaction with MuSK enabling downstream signaling transduction. The simulation methodology employed in this work may be readily applied to other peripheral membrane proteins. Alongside methods such as pMD-Membrane [40] which enable identification of possible ligand binding sites on membrane bound proteins, this computational approach may also facilitate discovery of druggable sites on protein/membrane complexes involved in membrane signaling pathways. In the context of Dok7, the characterization of the nature of PH-domain mediated targeting to cell membranes is a key first step in exploiting the nature of the Dok7/MuSK/membrane complex and its role in signaling.

Methods

Modelling of Dok7

The published structure of Dok7 (PDB id: 3ML4) was used as a starting point, using Modeller 9v8 [41] to model the missing unstructured regions between strands β1 and β2 in the PH domain.

CG-MD simulations

CG-MD simulations were performed using the MARTINI2.1 forcefield [42,43] with an elastic network (with a cutoff of 0.7 nm) applied to the protein. The protein was inserted into a box with a preformed bilayer of 356 lipids. The box was then solvated with CG water, and ions were added at physiological concentration (150 mM). Using a high-throughput approach, this was done 20 times, with the protein being placed in the box with a different orientation each time to ensure different initial configurations between the repeat simulations, and to ensure there was no bias in orientation of binding to the bilayer. These simulations were equilibrated then run for 1 μs each.

All CG-MD simulations were run with GROMACS 4.5.5 (www.gromacs.org) using the Berendsen thermostat and barostat for temperature and pressure coupling [44]. The LINCS algorithm was used to constrain bond length [45]. The integrator used was md, group neighbour lists were used, and Shift was used. Each simulation was equilibrated for 2.5 ns, then run using a time step of 20 fs at a temperature of 323 K. For each CG simulation, there was ~15,000 water particles in a box that was approximately 11 nm x 11 nm x 23.5 nm. CG to atomistic conversion was done using a fragment-based approach [46].

Calculation of density landscapes

To construct these density landscapes, we have merged all 20 simulations for each system. A two-dimensional histogram of R_{zz} and d_z was then derived from the ensemble of simulations, where d_z is the perpendicular distance between the centre of mass of the Dok7 PH domain and the centre of mass of the bilayer and R_{zz} is the zz component of the rotational matrix required for least squares fitting of an orientation onto a reference orientation. R_{zz} was calculated by using the g_rotmat command in GROMACS. The normalization of the 2-dimensional histogram was done by dividing each bin by the number of repeat simulations (20 for CG) multiplied by the total number of frames in each repeat simulation and by the bin area. After the calculation of the landscapes, the density in each bin was divided by the density in the global minimum to obtain normalized densities.

Atomistic MD simulations

Representative CG snapshots were chosen which corresponded to the distance and R_{zz} value of M1 from the coarse-grain simulations. Note that "distance" refers to the distance between the COM of the protein and the COM of the bilayer. These were then used as starting points for atomistic simulations. The AT model of the protein was generated from the CG model as described in Stansfeld *et al.* [46]. All simulations have been performed using the GROMOS96 43a1 force field [47]. The Parinello-Rahman barostat [48] and Berendsen thermostat [44] was used (T = 323 K), with the LINCS algorithm [45] used to constrain bond lengths. Particle Mesh Ewald (PME) [49] was used for long-range (cutoff = 1.2 nm) electrostatics. The simulation in a box size was 10.5 nm x 10.5 nm x 13.5 nm. Systems were equilibrated for 1 ns with the C_α atoms restrained (force constant 1000 kJ/mol/nm^2), followed by 300 ns of unrestrained simulations. Analysis was performed using GROMACS [37], VMD [50], and locally written scripts.

Supporting Information

S1 Fig. Coarse-grained structure of PI(4,5)P$_2$ and PI(3,4,5)P$_3$ molecules. Images of the coarse-grained models of the PI(4,5)P$_2$ **(A)** and PI(3,4,5)P$_3$ **(B)** lipids used in the simulations. The headgroups of the lipids are in van der Waals representation, whilst the tails are in licorice

representation. PI(4,5)P$_2$ is in purple, and PI(3,4,5)P$_3$ is in orange.
(TIF)

S2 Fig. Convergence analysis for Dok7 PH domain binding to PIP$_2$. Density landscapes for the CG-PH-pip2 system when it is separated into 4 x 5 µs, 2 x 10 µs and 1 x 20 µs densities.
(TIF)

S3 Fig. Lipid contact analysis between Dok7 and ASAP1. PIP binding sites observed in atomistic simulations of **(A)** Dok7; **(B)** ASAP1 (see [38] for details); and **(C)** a structural alignment of the two PH domains for comparison. Dok7 is in yellow cartoon, ASAP1 is in ochre cartoon, the PIP$_2$ that binds to Dok7 is in purple CPK and licorice, and the PIP$_2$ that binds to ASAP1 is in magenta CPK and licorice. This is further analysed by calculating averaged normalised lipid contacts for the simulations of **(D)** ASAP1 and **(E)** Dok7. The β1/ β2 and β3/ β4 loops are highlighted on the graphs with red lines, and the *canonical* and *atypical* sites are labelled with a "C" and "A" respectively.
(TIF)

S4 Fig. Dok7 PH domain's interactions with PIP$_2$ and PIP$_3$ lipids. Number of contacts of Dok7's PH domain with the headgroups **(A)**, phosphates **(B)**, and tails **(C)** of PIP$_2$, and the headgroups **(D)**, phosphates **(E)**, and tails **(F)** of PIP$_3$. PC and PS lipids are represented by either a red or green line, respectively; PIP$_2$ lipids are represented by a purple line, and PIP$_3$ lipids are represented by an orange line.
(TIF)

S5 Fig. Secondary structure analysis of Dok7 PH atomistic simulations. (A) Secondary structure analysis of all Dok7 PH atomistic simulations. Simulations containing PIP$_2$ are in the left column, whilst the simulations containing PIP$_3$ are in the right column. Each individual simulation is shown as a separate graph, with the different secondary structures highlighted in blue (α-helix), red (β-sheet), black (coil), green (bend), yellow (loop), orange (β bridge), purple (5-helix), and pink (3-helix). **(B)** Root mean square fluctuation (RMSF) of each residue on Dok7's PH domain for simulations with PIP$_2$ (left) and PIP$_3$ (right). Each replicate is shown in a different colour.
(TIF)

S6 Fig. Hydrogen bond analysis for Dok7 PH domain. Hydrogen bonds between the Dok7 PH domain with **(A)** PIP$_2$ (above) and **(B)** PIP$_3$ (below) from the three repeat atomistic simulations (rep1 to 3).
(TIF)

S7 Fig. Hydrogen bond analysis for key residues on Dok7 PH domain. Hydrogen bonds of selected residues (K18, K20, R22 and R54) on the Dok7 PH domain with PIP$_2$ **(A)** and PIP$_3$ **(B)**. The colours correspond to the three repeat atomistic simulations.
(TIF)

S8 Fig. Atomistic lipid contacts. Atomistic lipid contacts broken down into headgroup **(A)**, phosphates **(B)**, and tails **(C)** of PIP$_2$, and the headgroups **(D)**, phosphates **(E)**, and tails **(F)** of PIP$_3$. PC is shown in red, PS in green, PIP$_2$ in purple, and PIP$_3$ in orange.
(TIF)

S1 File. Structure of Dok7 PH domain with the lipid bilayer. PDB file of the Dok7 PH domain with a PC/PS/PIP$_2$ bilayer that is aligned with the Arf GAP ASAP1 structure.
(PDB)

Acknowledgments

We thank Dr. Eiji Yamamoto for providing access to his simulations of ASAP1 for comparison to Dok7.

Author Contributions

Conceived and designed the experiments: AB ACK MSPS. Performed the experiments: AB. Analyzed the data: AB ACK. Contributed reagents/materials/analysis tools: ACK. Wrote the paper: AB ACK MSPS.

References

1. Mashima R, Hishida Y, Tezuka T, Yamanashi Y. The roles of Dok family adapters in immunoreceptor signaling. Immunol Rev. 2009 Nov; 232(1):273–85. doi: 10.1111/j.1600-065X.2009.00844.x PMID: 19909370

2. Okada K, Inoue A, Okada M, Murata Y, Kakuta S, Jigami T, et al. The muscle protein Dok-7 is essential for neuromuscular synaptogenesis. Science. 2006 Jun 23; 312(5781):1802–5. PMID: 16794080

3. DeChiara TM, Bowen DC, Valenzuela DM, Simmons M V, Poueymirou WT, Thomas S, et al. The receptor tyrosine kinase MuSK is required for neuromuscular junction formation in vivo. Cell. 1996; 85 (4):501–12. PMID: 8653786

4. Kummer TT, Misgeld T, Sanes JR. Assembly of the postsynaptic membrane at the neuromuscular junction: Paradigm lost. Curr Opin Neurobiol. 2006; 16(1):74–82. PMID: 16386415

5. Wu H, Xiong WC, Mei L. To build a synapse: signaling pathways in neuromuscular junction assembly. Development. 2010; 137(7):1017–33. doi: 10.1242/dev.038711 PMID: 20215342

6. Hamuro J, Higuchi O, Okada K, Ueno M, Iemura S, Natsume T, et al. Mutations causing DOK7 congenital myasthenia ablate functional motifs in Dok-7. J Biol Chem. 2008 Feb 29; 283(9):5518–24. doi: 10.1074/jbc.M708607200 PMID: 18165682

7. Müller JS, Herczegfalvi A, Vilchez JJ, Colomer J, Bachinski LL, Mihaylova V, et al. Phenotypical spectrum of DOK7 mutations in congenital myasthenic syndromes. Brain. 2007 Jul; 130(Pt 6):1497–506. PMID: 17439981

8. Lorenzoni PJ, Scola RH, Kay CSK, Filla L, Miranda APP, Pinheiro JMR, et al. Salbutamol therapy in congenital myasthenic syndrome due to DOK7 mutation. J Neurol Sci. 2013; 331(1–2):155–7. doi: 10.1016/j.jns.2013.05.017 PMID: 23790237

9. Lashley D, Palace J, Jayawant S, Robb S, Beeson D. Ephedrine treatment in congenital myasthenic syndrome due to mutations in DOK7. Neurology. 2010 May 11; 74(19):1517–23. doi: 10.1212/WNL.0b013e3181dd43bf PMID: 20458068

10. Palace J, Lashley D, Newsom-Davis J, Cossins J, Maxwell S, Kennett R, et al. Clinical features of the DOK7 neuromuscular junction synaptopathy. Brain. 2007 Jul; 130(Pt 6):1507–15. PMID: 17452375

11. Yamanashi Y, Higuch O, Beeson D. Dok-7/MuSK signaling and a congenital myasthenic syndrome. Acta Myol. 2008 Jul; 27:25–9. PMID: 19108574

12. Palace J. DOK7 congenital myasthenic syndrome. Ann N Y Acad Sci. 2012 Dec 1; 1275(1):49–53.

13. Bergamin E, Hallock PT, Burden SJ, Hubbard SR. The cytoplasmic adaptor protein Dok7 activates the receptor tyrosine kinase MuSK via dimerization. Mol Cell. 2010 Jul 9; 39(1):100–9. doi: 10.1016/j.molcel.2010.06.007 PMID: 20603078

14. Lietzke SE, Bose S, Cronin T, Klarlund J, Chawla A, Czech MP, et al. Structural basis of 3-phosphoinositide recognition by pleckstrin homology domains. Mol Cell. 2000 Aug; 6(2):385–94. PMID: 10983985

15. Ferguson KM, Lemmon MA, Schlessinger J, Sigler PB. Structure of the High Affinity Complex of Inositol Trisphosphate with a Phospholipase C Pleckstrin Homology. 1995; 83:1037–46.

16. Milburn CC, Deak M, Kelly SM, Price NC, Alessi DR, van Aalten DMF. Binding of phosphatidylinositol 3,4,5-trisphosphate to the pleckstrin homology domain of protein kinase B induces a conformational change. Biochem J. 2003; 538:531–8.

17. Liu J, Fukuda K, Xu Z, Ma Y-Q, Hirbawi J, Mao X, et al. Structural basis of phosphoinositide binding to kindlin-2 protein pleckstrin homology domain in regulating integrin activation. J Biol Chem. 2011 Dec 16; 286(50):43334–42. doi: 10.1074/jbc.M111.295352 PMID: 22030399

18. Boulay I, Nemorin J-G, Duplay P. Phosphotyrosine Binding-Mediated Oligomerization of Downstream of Tyrosine Kinase (Dok)-1 and Dok-2 Is Involved in CD2-Induced Dok Phosphorylation. J Immunol. 2005 Sep 21; 175(7):4483–9. PMID: 16177091

19. Geer P Van Der, Pawson T. The PTB Domain: a new protein module implicated in signal transduction. Trends Biochem Sci. 1995; 20:277–80. PMID: 7545337

20. Hedger G, Sansom MSP, Koldsø H. The juxtamembrane regions of human receptor tyrosine kinases exhibit conserved interaction sites with anionic lipids. Sci Rep. 2015; 5:9198. doi: 10.1038/srep09198 PMID: 25779975

21. Kalli AC, Sansom MSP. Interactions of peripheral proteins with model membranes as viewed by molecular dynamics simulations. Biochem Soc Trans. 2014 Oct; 42(5):1418–24. doi: 10.1042/BST20140144 PMID: 25233425

22. Han DS, Golebiewska U, Stolzenberg S, Scarlata SF. A Dynamic Model of Membrane-Bound Phospholipase Cβ2 Activation by GβγSubunits. 2011; 80(3):434–45.

23. Lai C.L., Landgraph K.E., Voth G.A., Falke JJ. Membrane Docking Geometry and Target Lipid Stoichiometry of Membrane-Bound PKCα C2 Domain: A Combined Molecular Dynamics and Experimental Study. J Mol Biol. 2010; 402(2):301–10. doi: 10.1016/j.jmb.2010.07.037 PMID: 20659476

24. Kalli AC, Devaney I, Sansom MSP. Interactions of phosphatase and tensin homologue (PTEN) proteins with phosphatidylinositol phosphates: insights from molecular dynamics simulations of PTEN and voltage sensitive phosphatase. Biochemistry. 2014 Mar 25; 53(11):1724–32. doi: 10.1021/bi5000299 PMID: 24588644

25. Kalli AC, Morgan G, Sansom MSP. Interactions of the auxilin-1 PTEN-like domain with model membranes result in nanoclustering of phosphatidyl inositol phosphates. Biophys J. 2013 Jul 2; 105(1):137–45. doi: 10.1016/j.bpj.2013.05.012 PMID: 23823232

26. Kalli AC, Wegener KL, Goult BT, Anthis NJ, Campbell ID, Sansom MSP. The structure of the talin/integrin complex at a lipid bilayer: an NMR and MD simulation study. Structure. 2010 Oct 13; 18(10):1280–8. doi: 10.1016/j.str.2010.07.012 PMID: 20947017

27. Gorfe AA, Hanzal-bayer M, Abankwa D, Hancock JF, Mccammon JA. Structure and Dynamics of the Full-Length Lipid-Modified H-Ras Protein in a 1,2-dimyristoylglycero-3-phosphocholine bilayer. J Med Chem. 2007; 50:674–84. PMID: 17263520

28. Abankwa D, Hanzal-bayer M, Ariotti N, Plowman SJ, Gorfe AA, Parton RG, et al. A novel switch region regulates H-ras membrane orientation and signal output. EMBO J. 2008; 27(5):727–35. doi: 10.1038/emboj.2008.10 PMID: 18273062

29. Lumb CN, He J, Xue Y, Stansfeld PJ, Stahelin R V, Kutateladze TG, et al. Article Biophysical and Computational Studies of Membrane Penetration by the GRP1 Pleckstrin Homology Domain. Structure. 2011; 19(9):1338–46. doi: 10.1016/j.str.2011.04.010 PMID: 21893292

30. Jackson SG, Zhang Y, Haslam RJ, Junop MS. Structural analysis of the carboxy terminal PH domain of pleckstrin bound to D-myo-inositol 1,2,3,5,6-pentakisphosphate. BMC Struct Biol. 2007 Jan; 7:80. PMID: 18034889

31. Komander D, Fairservice A, Deak M, Kular GS, Prescott AR, Peter Downes C, et al. Structural insights into the regulation of PDK1 by phosphoinositides and inositol phosphates. EMBO J. 2004 Oct 13; 23 (20):3918–28. PMID: 15457207

32. Hall BA, Halim KA, Buyan A, Emmanouil B, Sansom MSP. A Sidekick for Membrane Simulations: Automated Ensemble Molecular Dynamics Simulations of Transmembrane Helices. J Chem Theory Comput. 2014; 10(5):2165–75. doi: 10.1021/ct500003g PMID: 26580541

33. Wassenaar TA, Pluhackova K, Moussatova A, Sengupta D, Marrink SJ, Tieleman DP, et al. High-Throughput Simulations of Dimer and Trimer Assembly of Membrane Proteins. The DAFT Approach. J Chem Theory Comput. 2015;May; 11(5);2278–91. doi: 10.1021/ct5010092 PMID: 26574426

34. Arai N, Akimoto T, Yamamoto E, Yasui M, Yasuoka K. Poisson property of the occurrence of flip-flops in a model membrane. J Chem Phys. 2014; 140(6):064901. doi: 10.1063/1.4863330 PMID: 24527934

35. Ulmschneider JP, Smith JC, White SH, Ulmschneider MB. In Silico Partitioning and Transmembrane Insertion of Hydrophobic Peptides Under Equilibrium Conditions. J Amer Chem Soc. 2011; 133 (39):15487–95.

36. Jian X, Tang W-K, Zhai P, Roy NS, Luo R, Gruschus JM, et al. Molecular Basis for Cooperative Binding of Anionic Phospholipids to the PH Domain of the Arf GAP ASAP1. Structure. 2015;Nov 3; 23 (11):1977–88. doi: 10.1016/j.str.2015.08.008 PMID: 26365802

37. Hess B, Uppsala S, Lindahl E. GROMACS 4 : Algorithms for Highly Efficient, Load-Balanced, and Scalable Molecular Simulation. J Chem Theory Comput. 2008; 4:435–47. doi: 10.1021/ct700301q PMID: 26620784

38. Yamamoto E, Kalli AC, Yasuoka K, Sansom MSP. Interactions of Pleckstrin Homology Domains with Membranes: Adding Back the Bilayer via High Throughput Molecular Dynamics. Structure. 2016; In Press.

39. Rosen SAJ, Gaffney PRJ, Spiess B, Gould IR. Understanding the relative affinity and specificity of the pleckstrin homology domain of protein kinase B for inositol phosphates. Phys Chem Chem Phys. 2012; 14(2):929–36. doi: 10.1039/c1cp22240f PMID: 22121510

40. Prakash P, Sayyed-Ahmad A, Gorfe AA. pMD-Membrane: A Method for Ligand Binding Site Identification in Membrane-Bound Proteins. PLoS Comput Biol. 2015; 11(10):e1004469. doi: 10.1371/journal.pcbi.1004469 PMID: 26506102

41. Fiser A, Sali A. MODELLER: Generation and refinement of Homology-Based Protein Structure Models. Methods Enzymol. 2003; 374:461–92. PMID: 14696385

42. Monticelli L, Kandasamy SK, Periole X, Larson RG, Tieleman DP, Marrink SJ. The MARTINI Coarse-Grained Force Field: Extension to Proteins. J Chem Theory Comput. American Chemical Society; 2008 May; 4(5):819–34.

43. de Jong DH, Singh G, Bennett WFD, Arnarez C, Wassenaar TA, Schäfer L V., et al. Improved Parameters for the Martini Coarse-Grained Protein Force Field. J Chem Theory Comput. American Chemical Society; 2013 Jan 8; 9(1):687–97.

44. Berendsen HJC, Postma JPM, van Gunsteren WF, DiNola A, Haak JR. Molecular dynamics with coupling to an external bath. J Chem Phys. 1984; 81(8):3684.

45. Hess B. P-LINCS: A Parallel Linear Constraint Solver for Molecular Simulation. J Chem Theory Comput. 2008 Jan; 4(1):116–22. doi: 10.1021/ct700200b PMID: 26619985

46. Stansfeld PJ, Sansom MSP. From Coarse Grained to Atomistic: A Serial Multiscale Approach to Membrane Protein Simulations. J Chem Theory Comput. 2011 Apr 12; 7(4):1157–66. doi: 10.1021/ct100569y PMID: 26606363

47. Scott WRP, Hünenberger PH, Tironi IG, Mark AE, Billeter SR, Fennen J, et al. The GROMOS Biomolecular Simulation Program Package. J Phys Chem A. 1999; 103(19):3596–607.

48. Parrinello M. Polymorphic transitions in single crystals: A new molecular dynamics method. J Appl Phys. 1981; 52(12):7182.

49. Essmann U, Perera L, Berkowitz ML, Darden T, Lee H, Pedersen LG. A smooth particle mesh Ewald method. JChemPhys. 1995; 103(November):31–4.

50. Humphrey W., Dalke A., Schulten K. VMD: Visual Molecular Dynamics. J Mol Graph. 1996; 14:33–8. PMID: 8744570